Available on CMS information server

CMS AN-2008/075

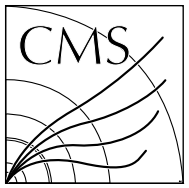

The Compact Muon Solenoid Experiment

Analysis Note

The content of this note is intended for CMS internal use and distribution only

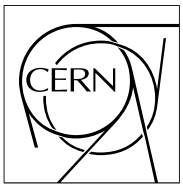

04 September 2008

Studies for photons and neutral pions identification in the ECAL barrel region

D. Franci, S. Rahatlou, D. del Re

Abstract

The neutral pions produced in jet fragmentation are a source of background for all the analyses with high-energy isolated photons in the final state. We present an algorithm using the moments of the energy distribution, to distinguish between unconverted photons and neutral pions in the ECAL barrel region. We have also investigated additional variables to increase the separation power by using a Fisher linear discriminant.

Contents

1 Introduction

Neutral pion decay $\pi^0 \rightarrow \gamma\gamma$ is an important source of background for all the analyses with high energy photons in the final state, such as the Higgs decay in the $\gamma\gamma$ channel. In fact, if the π^0 decay photons reach the CMS electromagnetic calorimeter (ECAL) in two points too close to each other, they can be detected as a single energy deposit and the π^0 can be misinterpreted as a photon of the same energy. For this reason, an algorithm to distinguish photons from neutral pions has a great importance for many of the primary goals of the LHC physics program.

Photons can be distinguished from neutral pions using the fine granularity of the ECAL crystals in the barrel region ($|\eta| < 1.497$). The geometrical properties of the electromagnetic energy deposits are described by variables commonly referred as *cluster shape variables*. These variables are used to identify the differences between the shape of γ and π^0 clusters. The endcap region won't be discussed in this note. We only remark that the $\gamma - \pi^0$ separation in this region is performed by the *preshower* detector [1], a position-sensitive device with high granularity.

In this note we present an optimized γ - π^0 discrimination algorithm for the barrel region. We implement a new set of cluster shape variables based on the moments of the energy distribution in the ECAL. We also combine moments with other cluster shape variables to improve the discrimination power. Only unconverted photons are currently being considered in this study.

This note is organized as follows: data set and analysis procedure are described in Section 2. Section 3 describes the moments of energy distribution calculated along the principal axes. In Section 4 we introduce other cluster shape variables and discuss the γ-π^0 discrimination algorithm. We summarize and conclude in Section 5.

2 Data Set and Analysis Procedure

Our data set consists of 150K single γ and 150K single π^0, generated with the CMS particle gun. Particles are generated with energy uniformly distributed between 30 GeV and 70 GeV, within the barrel region and reconstructed with a 9×9 matrix around the most energetic crystal of the event. Only the crystals inside this matrix are considered for cluster shape studies.

2.1 Distance δ between decay photons

Figure 1 shows a sketch of a $\pi^0 \rightarrow \gamma\gamma$ decay, emphasizing the distance δ between the impact points of the decay photons on the ECAL surface. This variable is strongly correlated with the shape of a π^0 cluster. Figure 2 shows

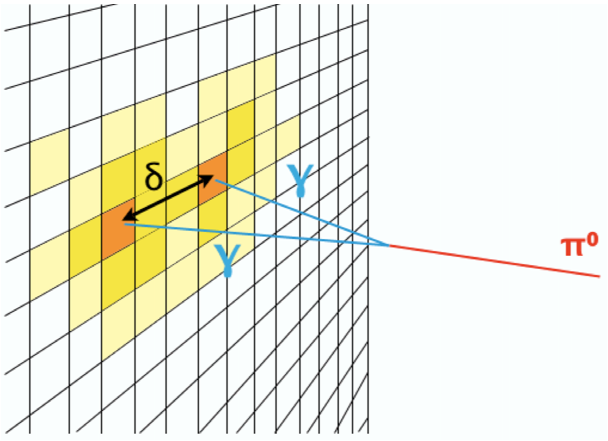

Figure 1: Sketch of a $\pi^0 \rightarrow \gamma\gamma$ decay. The distance between the impact points of the decay photons on the ECAL surface is referred as δ.

different topologies of π^0 energy deposits, corresponding to different values of δ:

$\delta = 6$ **cm:** When δ is several times the size of an ECAL crystal (2.2 cm), the decay photons are well separated and the π^0 can be easily recognized by computing the invariant mass (Figure 2a);

$\delta = 2$ **cm:** When δ is comparable with the size of a crystal, the decay photons are reconstructed as two overlapping clusters. In this case, the invariant mass cannot be computed with high precision but we can still recognize

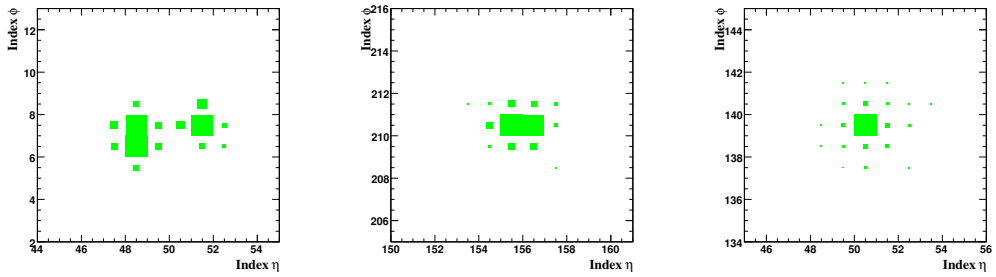

(a) (b) (c)

Figure 2: Distribution of energy deposit for neutral pions with: a) $\delta = 6$ cm; b) $\delta = 2$ cm; c) $\delta = 0.5$ cm. Each square represents a barrel crystal. Square's area is proportional to crystal energy.

the π^0 by the elliptical shape of its energy deposit (Figure 2b)

$\delta = 0.5$ **cm:** When δ is lower than the size of a crystal, the impact point of both photons is within the same crystal. The clusters are so overlapping that a π^0 cannot be distinguished from a single photon (Figure 2c).

An approximate expression for δ is:

$$\delta \sim 2 \cdot L\left(\eta_{\pi^0}\right) \cdot \tan \frac{\alpha\left(E_1, E_2\right)}{2} \tag{1}$$

where L is the distance between π^0 decay vertex and the point on ECAL surface corresponding to the π^0 pseudo-rapidity η_{π^0} and α is the angle between the directions of the decay photons. E_1 and E_2 are the energies of the decay photons.

Starting from Eq. 1, we look for an estimate of δ based only on reconstructed quantities. The distance L can be computed from the pseudo-rapidity of reconstructed cluster η_{RECO}, according to the following expression:

$$L\left(\eta_{RECO}\right) = \frac{L\left(0\right)}{\sin\left[\theta\left(\eta_{RECO}\right)\right]} \tag{2}$$

where $L\left(0\right) = 1.29$ m, i.e. the radius of the CMS electromagnetic calorimeter and $\theta\left(\eta_{RECO}\right)$ is the polar angle associated to η_{RECO}.

The angle α is obtained from the general expression for the decay angle:

$$\sin^2\left(\frac{\alpha}{2}\right) = \frac{M_{\pi^0}^2}{4E_1E_2} \tag{3}$$

However, α cannot be computed with high precision. In fact the energies of individual photons E_1 and E_2 are determinated with large uncertainties, due to the difficulties in distinguishing between two overlapping photons. To avoid this problem, we consider α_{MIN}, that is the decay angle when the pion energy is equally distributed between the two photons. The expression for α_{MIN} is:

$$\sin^2\left(\frac{\alpha_{MIN}}{2}\right) = \left(\frac{M_{\pi^0}}{E_{RECO}}\right)^2 \tag{4}$$

obtained by replacing $E_1 = E_2 = \frac{E_{RECO}}{2}$ in Eq. 3, where E_{RECO} is the pion reconstructed energy. The minimum angle α_{MIN} depends only on the pion energy that, unlike E_1 and E_2, is always well measured. As shown in Figure 3, α_{MIN} and α (obtained from Monte Carlo information) exhibit a linear correlation. The use of α_{MIN} instead of α is a reasonable approximation.

For each 9×9 matrix we can compute an estimate of δ (in the hypothesis of a π^0) by replacing $L\left(\eta_{\pi^0}\right)$ and $\alpha\left(E_1, E_2\right)$ with the reconstructed quantities defined in Eq. 2 and 4:

$$\delta_{EST}\left(\eta_{RECO}, E_{RECO}\right) = 2 \cdot L\left(\eta_{RECO}\right) \cdot \tan \frac{\alpha_{MIN}\left(E_{RECO}\right)}{2} \tag{5}$$

The shape of a π^0 cluster is correlated with δ_{EST}. All the cluster shape variables introduced in the next sections to describe the geometrical properties of electromagnetic deposits also depend on δ_{EST}. In order to maximize the discriminating power between photons and neutral pions, our samples are splitted into different categories of δ_{EST}.

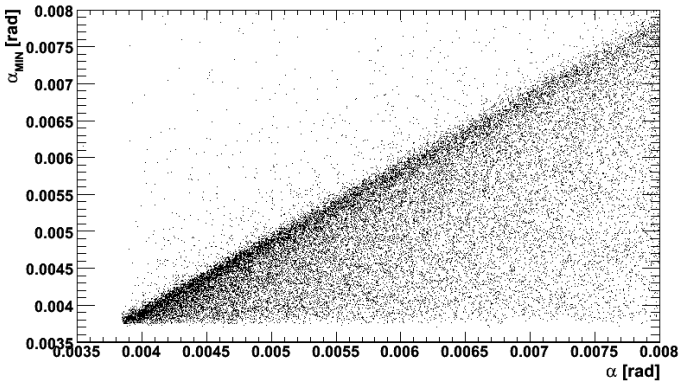

Figure 3: Minimum decay angle α_{MIN} for π^0, as a function of α.

3 Moments of energy distribution

A cluster is basically a spatial distribution (in the η-ϕ plane) of the energy deposit in the ECAL crystals. Like every other bidimensional distribution, a cluster can be described by its moments with respect to the *major* and *minor axes*, defined as the eigenvectors of the covariance matrix

$$COV_{\eta\phi} = \begin{pmatrix} S_{\eta\eta} & S_{\eta\phi} \\ S_{\phi\eta} & S_{\phi\phi} \end{pmatrix} \tag{6}$$

with

$$S_{\mu\nu} = \sum_{i=1}^{N} w_i \left(\mu_i - \langle\mu\rangle\right)\left(\nu_i - \langle\nu\rangle\right) \tag{7}$$

where N is the number of crystals in the cluster, μ_i and ν_i are the η, ϕ indices that identify the i-th crystal of the cluster and $\langle\mu\rangle = \frac{\sum_i w_i \cdot \mu_i}{\sum_i w_i}$. The weight w_i

$$w_i = max\left[4.2 + log\left(\frac{E_i}{E_{RECO}}\right); 0\right] \tag{8}$$

is the same used to calculate the position of a cluster [1]. The covariance matrix has already been used to provide a quantitative description of non-pointing photon signature [2].

Major and minor axes correspond to the directions along which the standard deviation of the energy distribution is respectively largest and lowest. Moments of order n are defined as

$$M^n_{MAJ(MIN)} = \frac{\sum_{i=1}^{N} w_i \left(d_i^{MIN(MAJ)}\right)^n}{\sum_{i=1}^{N} w_i} \tag{9}$$

where d_i^{MAJ} (d_i^{MIN}) is the distance between the center of the i-th crystal and the major (minor) axis, expressed in terms of η,ϕ indices. In the following we focus on the second-order moments since they have the highest γ-π^0 discrimination power. Moments with $n > 2$ are strongly correlated with second-order moments and therefore they are useless. Figure 4 shows a π^0 cluster with $\delta = 6$ cm. Lines represent major and minor axis, and their length corresponds to M^2_{MAJ} and M^2_{MIN} value.

Figure 5 shows the distribution of the average value of M^2_{MAJ} for photons and neutral pions, as a function of δ_{EST}. For pions, M^2_{MAJ} increases with larger values of δ_{EST}, since the energy deposit has a greater spread along the direction of the major axis. For photons, instead, M^2_{MAJ} is quite independent on δ_{EST}. For this reason, M^2_{MAJ} is a very powerful variable to distinguish between photons and pions. On the contrary, the energy distributions for photons and neutral pions along the minor axis are very similar to each other, regardless of the value of δ_{EST}: in other words, M^2_{MIN} is connected to the electromagneticity of a reconstructed cluster. As shown in Figure 6, M^2_{MIN} has no discriminating power between photons and neutral pions, so it is not used in this study. However, M^2_{MIN} can have other applications of interest. It could be used, for example, to distinguish between electromagnetic and hadronic clusters (jets).

Figure 7 shows M^2_{MAJ} distributions for photons and neutral pions with 0.8 cm $< \delta_{EST} < 1$ cm. Figure 8 gives

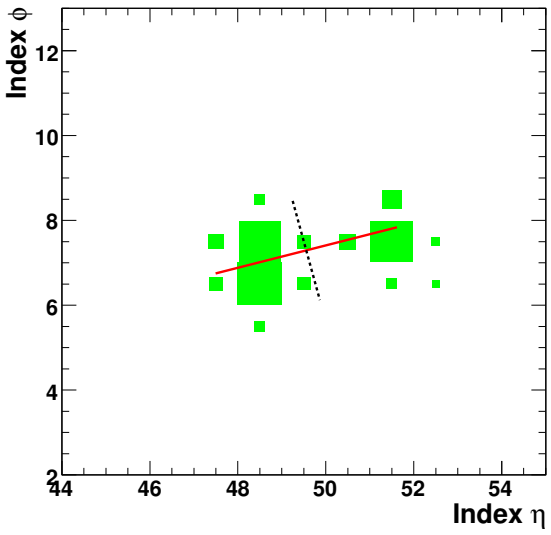

Figure 4: Distribution of energy deposit for a π^0 with $\delta = 6$ cm, overlaid with the major (solid line) and minor (dotted line) axes.

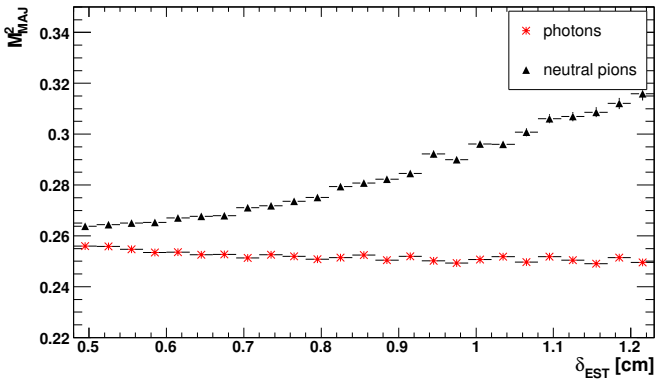

Figure 5: Distribution of the average value of M^2_{MAJ} for γ and π^0, as a function of δ_{EST}.

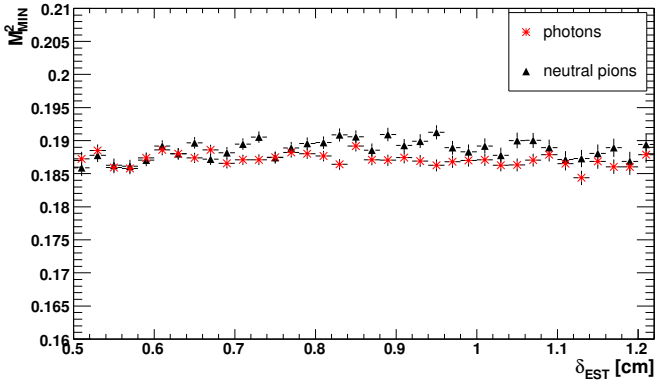

Figure 6: Distribution of the average value of M^2_{MIN} for γ and π^0, as a function of δ_{EST}.

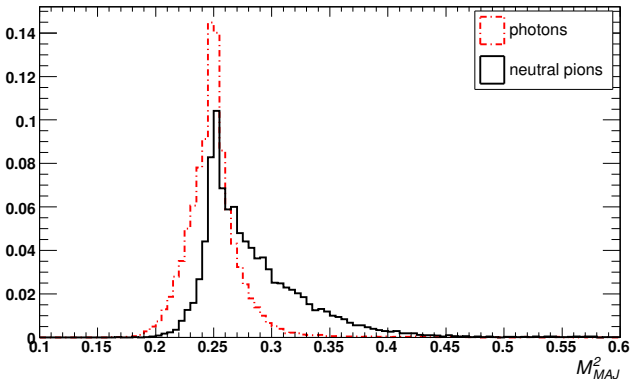

Figure 7: Distribution of M^2_{MAJ} for events with $0.8 < \delta_{EST} < 1$ cm.

the correlation between the neutral pion energy and δ_{EST}, showing that the values of δ_{EST} taken into account correspond to a large fraction of the photon energies expected from Higgs decay. In the following we will focus only on those clusters with 0.8 cm $< \delta_{EST} < 1$ cm. In Section 4.3 other bins of δ_{EST} will be considered.

The discrimination power of M^2_{MAJ} is summarized in the γ-identification efficiency vs π^0-rejection curve shown in Figure 9. Efficiency and rejection are calculated by selecting the events fulfilling the requirement $M^2_{MAJ} < M_{CUT}$ and varying the value of M_{CUT}. We note that M^2_{MAJ} has a very good discrimination power, even if δ_{EST} is so small. In fact, for an efficiency of photon identification of 80%, the pion rejection is about 60%.

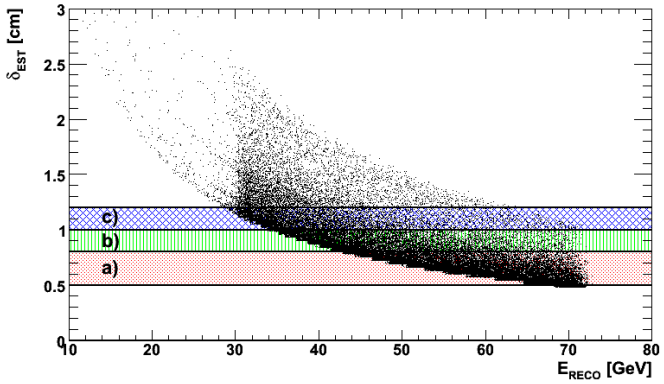

Figure 8: Estimated separation δ_{EST} for neutral pions, as a function of reconstructed energy E_{RECO}. The regions that will be considered in this note are indicated as: a) $0.5 < \delta_{EST} < 0.8$ cm; b) $0.8 < \delta_{EST} < 1$ cm; c) $1.0 < \delta_{EST} < 1.2$ cm.

4 Improve discrimination power combining different cluster shape variables

In this section we investigate an improved π^0-γ discriminating algorithm, by combining other variables with M^2_{MAJ}. We consider two additional cluster shape variables: the lateral moment LAT and the Zernike moments.

4.1 Lateral moment LAT

The lateral moment LAT was introduced by the Argus collaboration to separate electrons from hadrons [3]. LAT is defined as

$$LAT = \frac{\sigma_r^2}{\sigma_r^2 + E_1 + E_2} \tag{10}$$

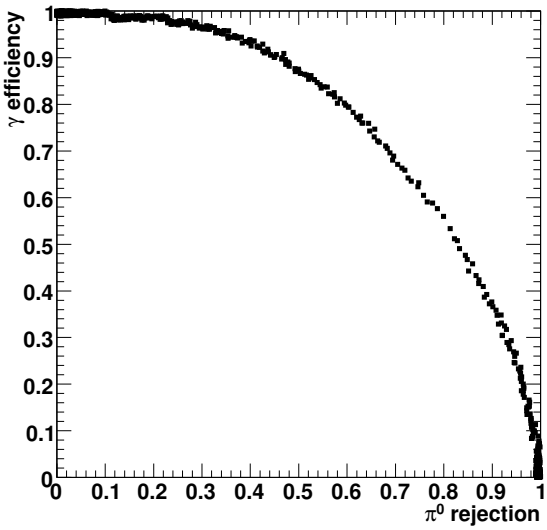

Figure 9: Efficiency of photon identification vs π^0 rejection for M^2_{MAJ}.

where E_1 and E_2 are the energies of the two most energetic crystals of the cluster and σ_r^2 has the following expression

$$\sigma_r^2 = \sum_{i=3}^{N} \frac{(\vec{r_i} - \vec{r})^2 E_i}{r_M^2} \tag{11}$$

where $\vec{r_i}$ is the radius vector of the i-th crystal, $\vec{r}$ is the radius vector of the cluster centroid and r_M is the Moliere radius of the electromagnetic calorimeter (2.2 cm for $PbWO_4$). Note that the two most energetic crystals are left out of the sum in Eq. 11. As shown in Figure 10, neutral pions have a lateral moment greater than photons. This was easily expected: most of the photon energy is indeed deposited in the two central crystals, while the pion energy is spread over a larger number of crystals.

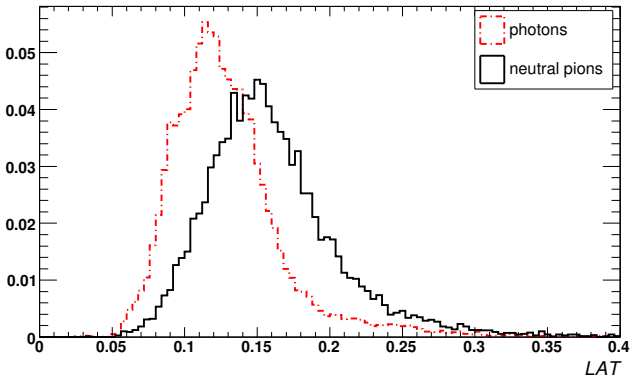

Figure 10: Distribution of LAT

4.2 Pseudo-Zernike moments

Another cluster shape variable is computed from the pseudo-Zernike moments, which are a set of polynomials that forms an orthonormal base on the unitary circle. These moments were used by Zeus collaboration [4] to identify electromagnetic particles, exploiting their showering properties within the electromagnetic calorimeter. The pseudo-Zernike moments A_{nm} are defined as

$$A_{nm} = \frac{n+1}{\pi} \sum_{i=1}^{N} \frac{E_i}{E_{TOT}} V_{nm}^{*}(\rho_i, \phi_i) \tag{12}$$

where n and m are two integers. The complex polynomials $V^*_{nm}(\rho_i, \phi_i)$, expressed in polar coordinates, are defined as

$$V^*_{nm}(\rho_i, \phi_i) = \sum_{s=0}^{\frac{n-m}{2}} \frac{(-1)^s (m-s)!}{s!(\frac{n+m}{2}-s)!(\frac{n-m}{2}-s)!} \rho_i^{m-2s} \cdot \exp^{-im\phi_i} \tag{13}$$

The cluster shape variable PZM used in this study is computed as

$$PZM = \sqrt{Re^2\left(A_{20}\right) + Im^2\left(A_{20}\right)} \tag{14}$$

i. e. the norm of the A_{20} moment. The distributions of PZM for photons and pions are shown in Figure 11.

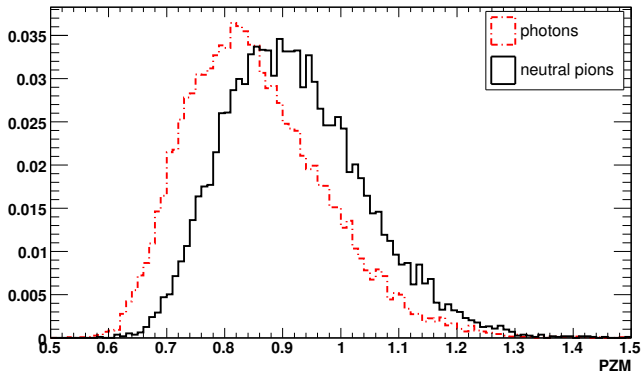

Figure 11: Distribution of PZM

4.3 Combination of different discriminants

Figure 12 shows a comparison between the γ-identification efficiency vs π^0-rejection curves for M^2_{MAJ}, LAT and PZM. It can be seen that M^2_{MAJ} provides the best separation power for any value of photon efficiency. In this section we present a simple algorithm that uses the other variables to improve M^2_{MAJ} stand-alone performance. We use the Fisher linear discriminant method, which is used to maximize the separation between two samples,

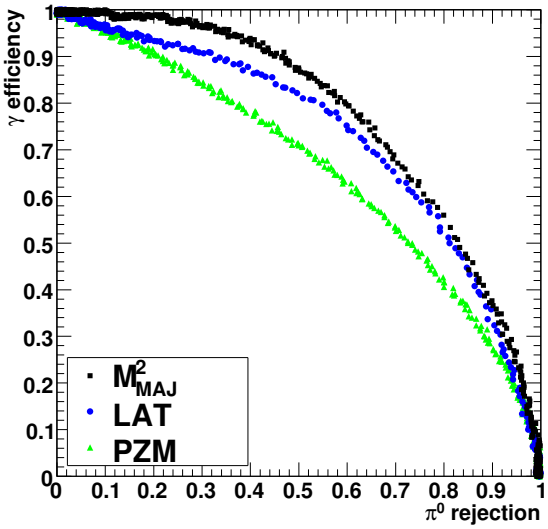

Figure 12: Efficiency of photon identification vs π^0 rejection for M^2_{MAJ}, LAT and PZM.

usually signal and background. We combine the cluster shape variables in a Fisher linear discriminant Y, defined as

$$Y = \sum_i a_i \cdot x_i \tag{15}$$

where x_i are the input variables and a_i are the Fisher coefficients, obtained using the training samples of photons and neutral pions described in Section 2. The original definition of the Fisher linear discriminant can be found in Ref. [5].

We combine M^2_{MAJ} with the other two variables in a Fisher discriminant to determine the combination which provides the best separation power. Figure 13 shows that any combination is worse than M^2_{MAJ} alone. This happens because the Fisher linear discriminant does not work well when the input variables are not gaussian. This is the case for M^2_{MAJ}, whose distribution is shown in Figure 7.

Then we use M^2_{MAJ} separately and combine LAT and PZM in a Fisher discriminant Y^*. The distributions of Y^* for photons and neutral pions are shown in Figure 14. Finally, the selection based only on M^2_{MAJ} is compared

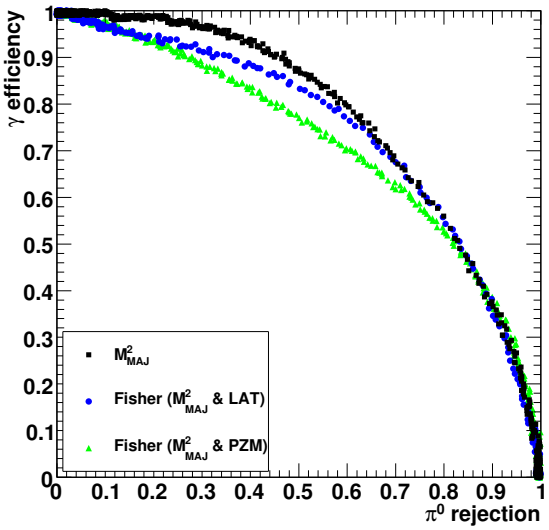

Figure 13: Efficiency of photon identification vs π^0 rejection for Fisher discriminants containing M^2_{MAJ}.

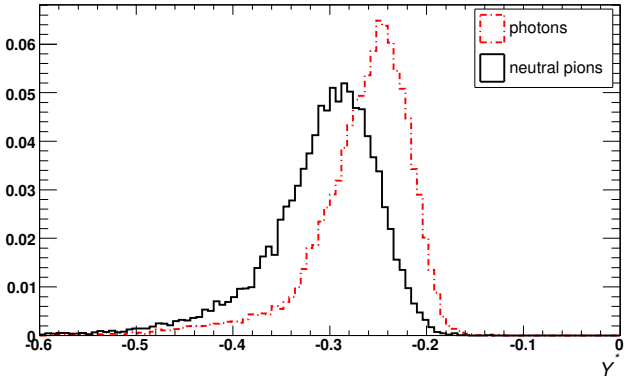

Figure 14: Distribution of Y^*.

with the performance of a selection on both M^2_{MAJ} and Y^* ($M^2_{MAJ} < M_{CUT}$ and $Y^* > Y^*_{CUT}$). For a given value of γ-identification efficiency, we vary the value of M_{CUT} and Y_{CUT} in order to maximize the pion rejection. The results of this selection are reported in Figure 15 and compared with the selection on M^2_{MAJ}. We note that the usage of both M^2_{MAJ} and Y^* separately provides a better discriminating power than using M^2_{MAJ} only.

The same procedure can be repeated for different bins of δ_{EST}. Figures 16a) and 16b) show the performance of the optimized selection criterion respectively for 0.5 cm $< \delta_{EST} < 0.8$ cm and 1.0 cm $< \delta_{EST} < 1.2$ cm. Note that, as δ_{EST} increases, M^2_{MAJ} become more and more powerful than Y^*: for $\delta_{EST} > 1.0$ cm, the selection criterion based only on M^2_{MAJ} is equivalent to the optimized one.

Figure 17 shows a comparison between the optimized selection criterion and the selection based only on M^2_{MAJ}.

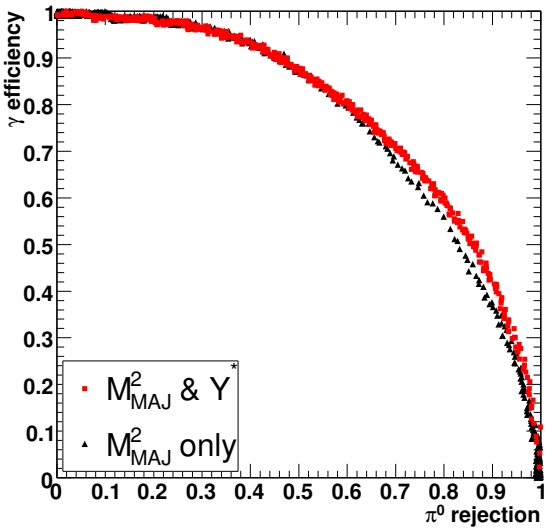

Figure 15: Efficiency of photon identification vs π^0 rejection for M^2_{MAJ} and the optimized selection criterion.

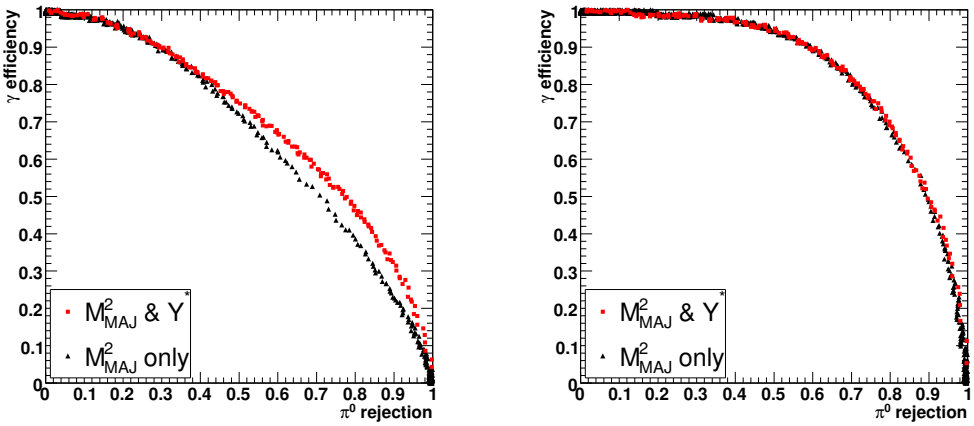

(a) (b)

Figure 16: Efficiency of photon identification vs π^0 rejection for M^2_{MAJ} and the optimized selection criterion, for different categories of δ_{EST}: a) $0.5 < \delta_{EST} < 0.8$ cm; b) $1.0 < \delta_{EST} < 1.2$ cm.

It includes all the categories of δ_{EST} previously considered and the selection is optimized separately for each of them. The number of photons and neutral pions is the same in each category. It can be seen that the optimized selection improves the separation power in the region of high π^0 rejection. For low values of π^0 rejection, instead, the two selections are equivalent.

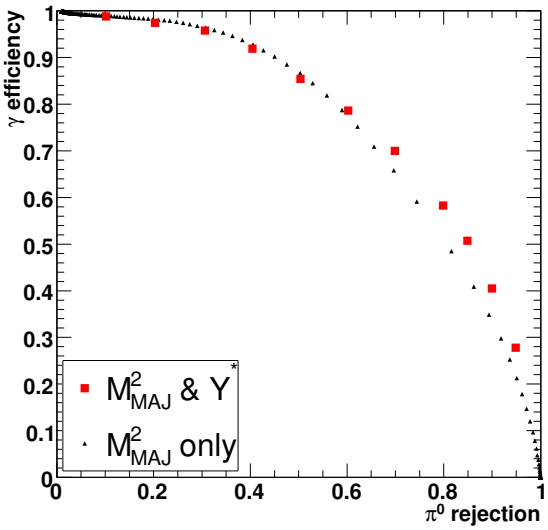

Figure 17: Efficiency of photon identification vs π^0 rejection for M^2_{MAJ} and the optimized selection criterion, including the categories of δ_{EST} previously considered. The selection is optimized separately for each category. The red points are obtained with the same number of photons and neutral pions in each category.

5 Conclusions

We presented an algorithm to distinguish between unconverted photons and neutral pions in the ECAL barrel region, using a new set of variables based on the moments of the energy distribution. The moments have been compared with other variables already implemented and used for cluster shape studies. We studied these variables as a function of the estimated distance between the impact points of pion's decay photons δ_{EST}, which is strongly correlated with the shape of a π^0 cluster. The second moment along the major axis M^2_{MAJ} is the most powerful variable to distinguish between photons and neutral pions. On the contrary, the second moment along the minor axis M^2_{MIN} has no discriminating power. However it could be used to distinguish between electromagnetic and hadronic clusters. Finally, we tried to increase the discriminating power by studying different combination of M^2_{MAJ} with the lateral moment LAT and the pseudo-Zernike moment PZM. We found that the best selection uses M^2_{MAJ} together with a Fisher linear discriminant which combines LAT and PZM.

References

[1] The CMS Collaboration, *CMS Physics TDR, Volume*, CERN-LHC-2006-001 (2006).

[2] G. Franzoni, *The electromagnetic calorimeter of CMS and its sensitivity to non-pointing photons*, PhD thesis.

[3] Argus coll., Nucl. Instrum. Meth. A **237** (1985) 464.

[4] R. Sinkus and T. Voss, Nucl. Instrum. Meth. A **389** (1997) 160.

[5] R.A. Fisher, *The use of multiple measures in taxonomic problems*, Ann. Eugenics, vol. 7 (1936) 179.